

# Supporting Information

## High-Loading Single-Atom Chromium Catalysts on Graphullerene for Oxygen Reduction Reactions

Jing Wang<sup>1</sup>, Xiaoyan Ren<sup>1</sup>, Shunfang Li<sup>1</sup>, Yuanyuan Shang<sup>1</sup> \*, Rui Pang<sup>1</sup> \*

<sup>1</sup>School of Physics and Laboratory of Zhongyuan Light, Zhengzhou University,

Zhengzhou 450052, China

Corresponding author: Yuanyuan Shang, Rui Pang

E-mail address: [yuanyuanshang@zzu.edu.cn](mailto:yuanyuanshang@zzu.edu.cn), [pangrui@zzu.edu.cn](mailto:pangrui@zzu.edu.cn)

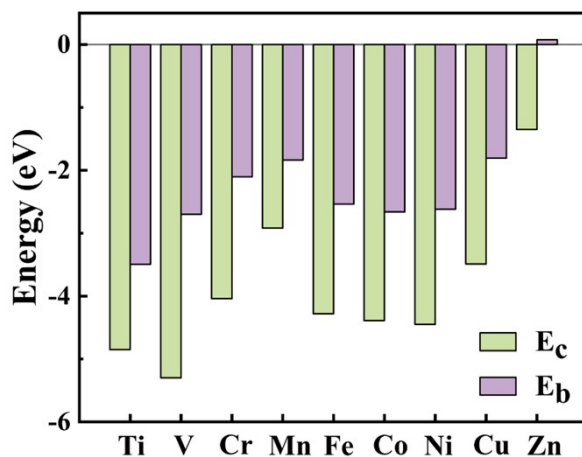


**Figure S1.** The binding energy ( $E_b$ ) and cohesion energy ( $E_c$ ) of TM-loaded graphullerene.  $E_c$  are the experimental values.<sup>1-2</sup>

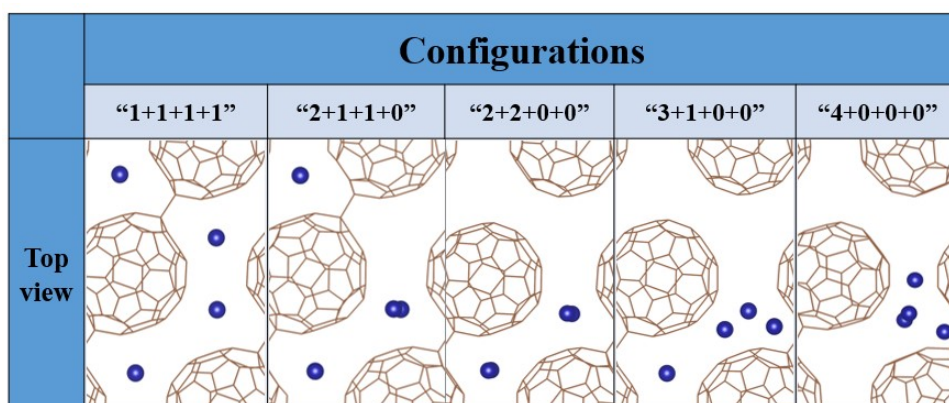


**Figure S2.** Optimized configurations of four Cr atoms loaded on graphullerene (including atomic dispersion, dimers, trimers and tetramers).

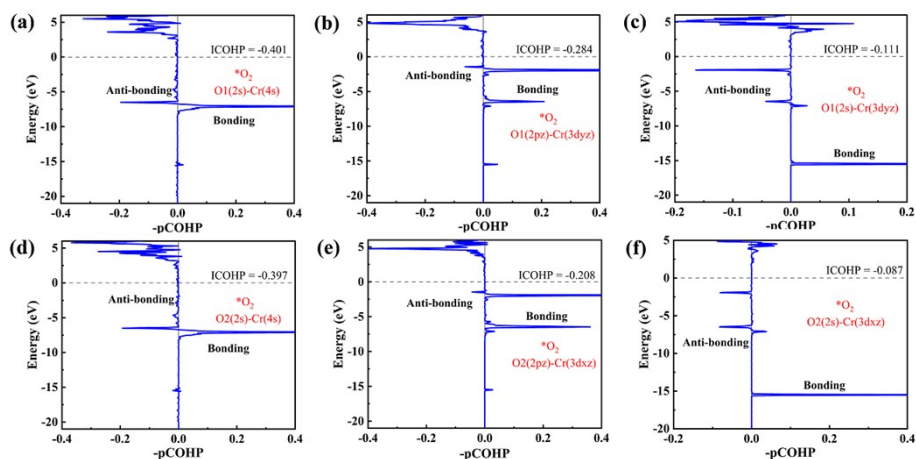


**Figure S3.** The COHP diagram (with specific orbital contributions) of Cr-O bond for O<sub>2</sub> adsorbed on the Cr@gra structure.

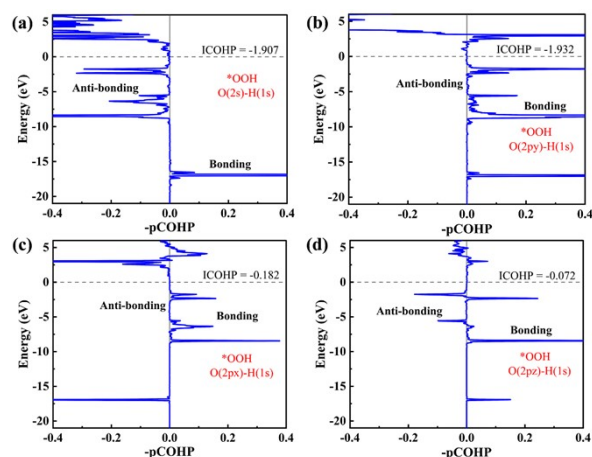


**Figure S4.** The COHP diagram (with specific orbital contributions) of O-H bond for OOH adsorbed on the Cr@gra structure.

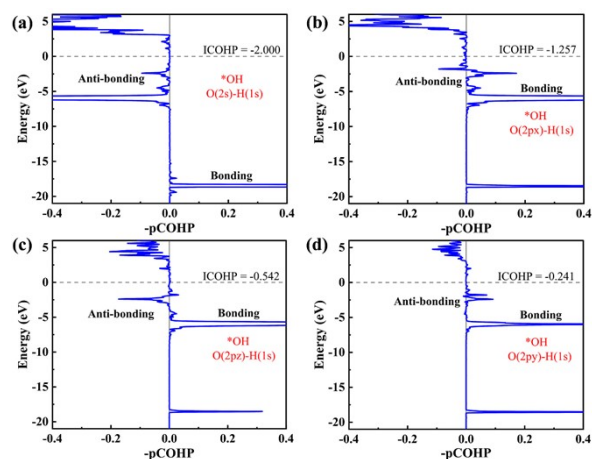


**Figure S5.** The COHP diagram (with specific orbital contributions) of O-H bond for OH adsorbed on the Cr@gra structure.

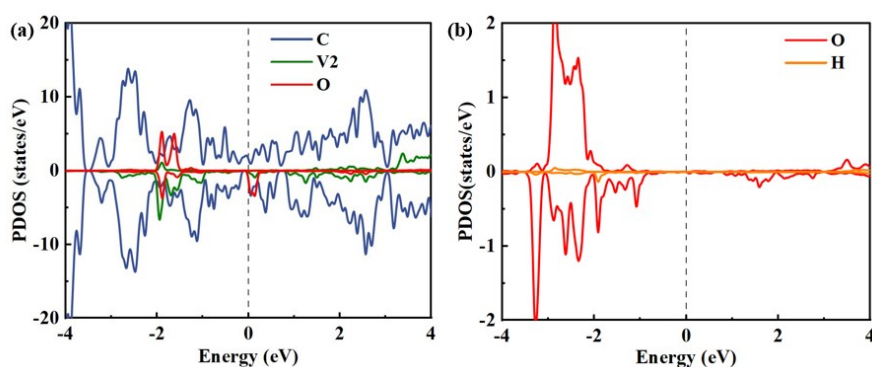


**Figure S6.** (a) (b) The PDOS of the corresponding atoms after intermediates (\*O<sub>2</sub> and \*OH) adsorption on V@gra.

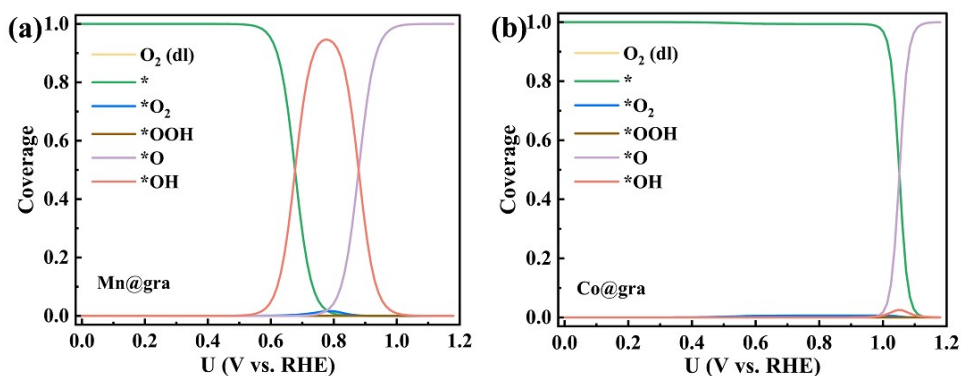


**Figure S7. (a) (b)** Microkinetic model simulated species coverage as a function of electrode potential on Mn@gra and Co@gra model.

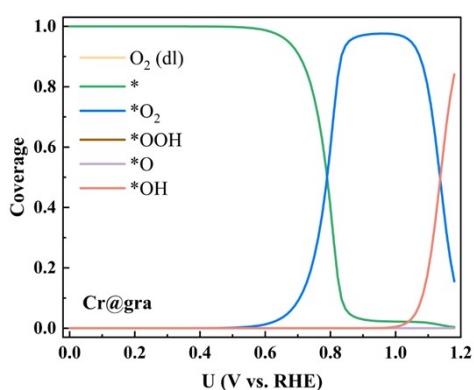


**Figure S8.** Microkinetic model simulated species coverage as a function of electrode potential on Cr@gra model.

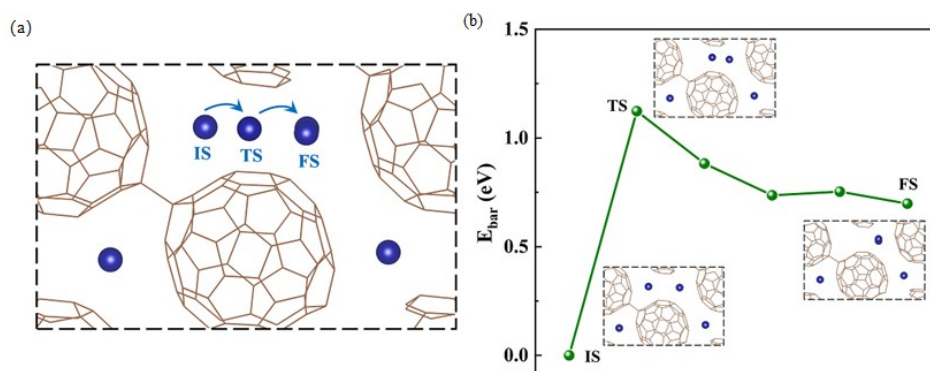


**Figure S9. (a)** Minimum energy path for Cr atom diffusion between dispersed configuration (IS) and dimeric configuration (FS) (TS is transition state) and **(b)** activation energy barrier ( $E_{\text{bar}}$ ).

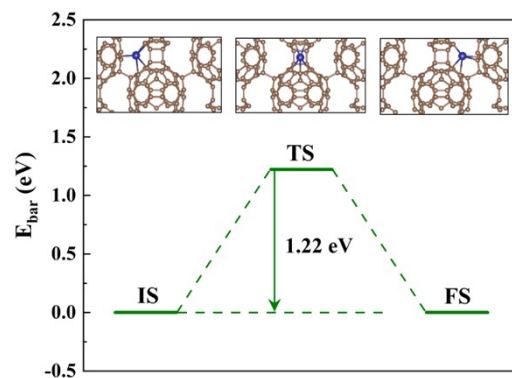


**Figure S10.** Activation energy barrier ( $E_{\text{bar}}$ ) in the minimum-energy path for a single Cr atom diffusion between two neighboring sites on graphullerene.

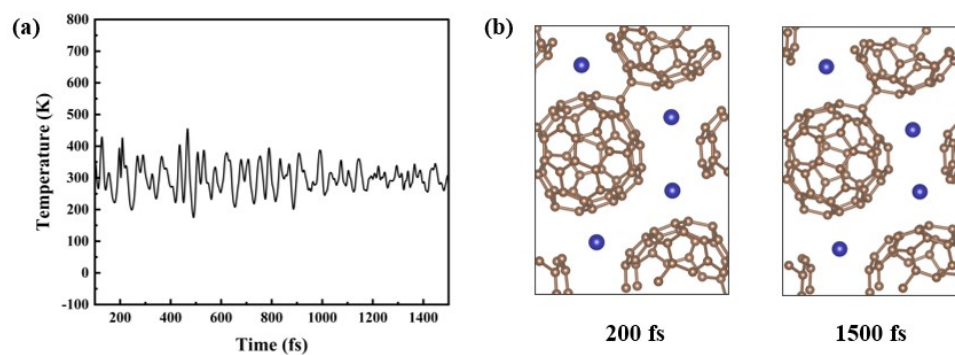


**Figure S11.** (a) Thermodynamic stability of the Cr@gra was examined by ab initio molecular dynamics simulations performed at 300 K with a time-step of 1 fs. (b) Representative snapshots of the geometric structures are presented.

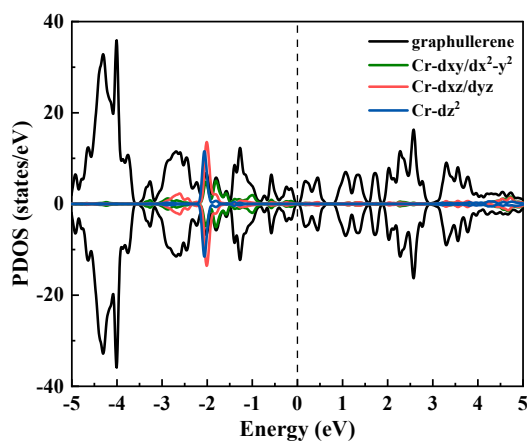


**Figure S12.** The projected density of states (PDOS) of graphullerene substrate and Cr atoms in the Cr@gra system.

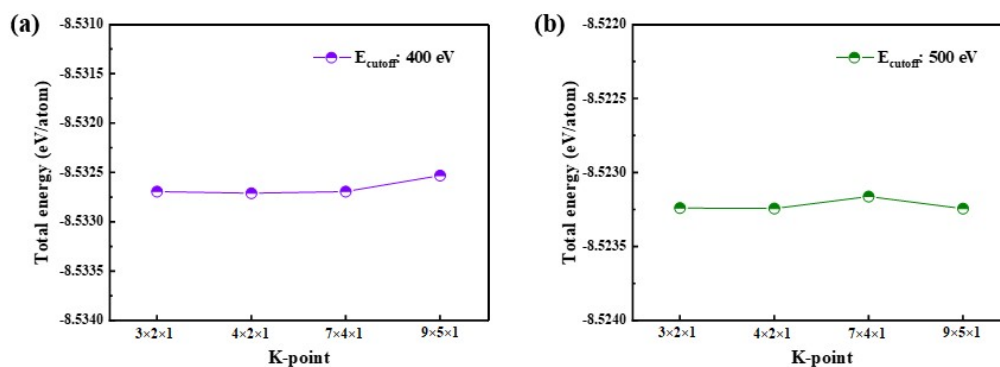


**Figure S13.** Total energy per atom (eV/atom) as a function of K-point size for plane-wave cutoff energies of (a) 400 eV and (b) 500 eV.

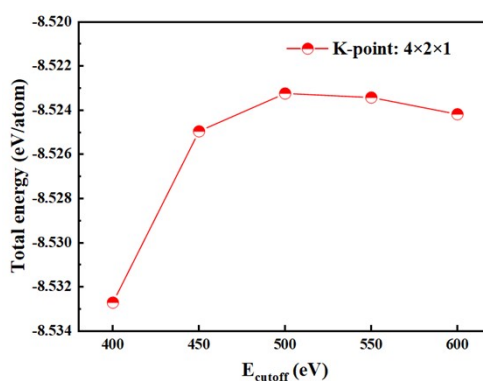


**Figure S14.** Total energy per atom (eV/atom) as a function of the cutoff energy ( $E_{\text{cutoff}}$ ) for a K-point of  $4 \times 2 \times 1$ .

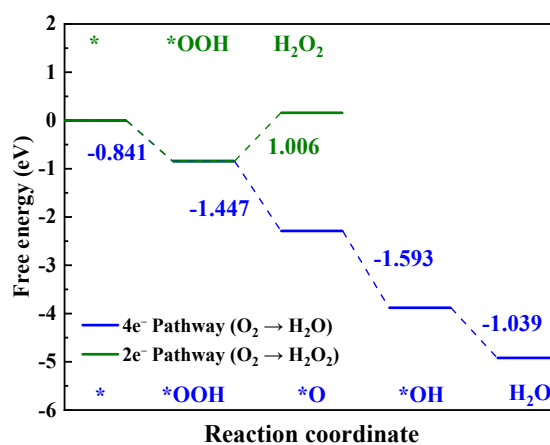


**Figure S15.** Free energy diagram of the 4-electron ( $\text{O}_2 \rightarrow \text{H}_2\text{O}$ ) and 2-electron ( $\text{O}_2 \rightarrow \text{H}_2\text{O}_2$ ) pathways for the ORR.

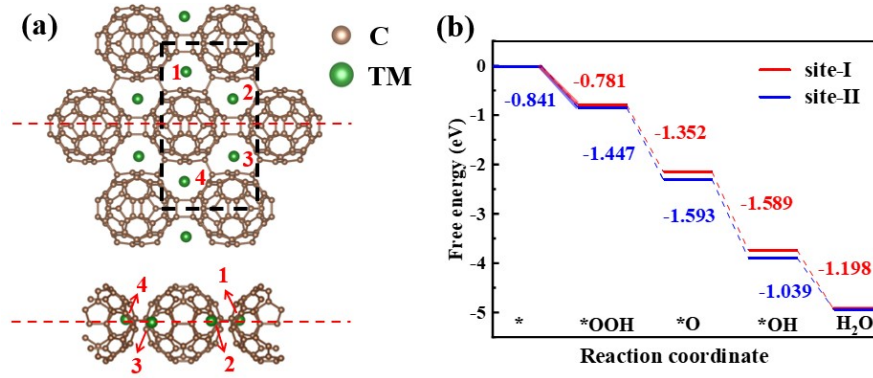


**Figure S16.** (a) Top view and side view of TM@gra system. (b) Free energy diagram for ORR on site-I and site-II of the Cr@gra system.

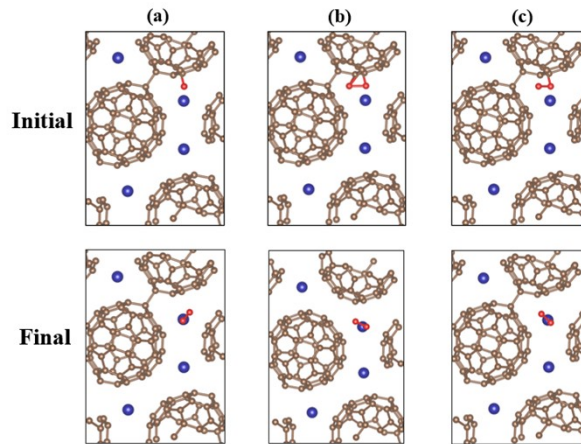


**Figure S17.** Initial and final optimized adsorption configurations of  $\text{O}_2$  adsorption on Cr@gra with various typical adsorption orientations.

## ORR free energy calculations

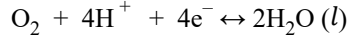
The Gibbs free energy change ( $\Delta G$ ) is calculated using computational hydrogen electrode (CHE) method developed by Nørskov et al,<sup>3</sup> as follows:

$$\Delta G = \Delta E_{\text{DFT}} + \Delta E_{\text{ZPE}} - T\Delta S + \Delta G_{\text{pH}} + \Delta G_{\text{U}} \quad (\text{S1})$$

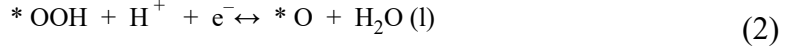
Where  $\Delta E_{\text{DFT}}$ ,  $\Delta E_{\text{ZPE}}$ , and  $\Delta S$  represent the difference of energy between reactants and products, the zero-point energy correction, and the change in entropy, respectively,  $\Delta G_{\text{pH}} = k_{\text{B}} T \ln 10 \times \text{pH}$  ( $k_{\text{B}}$ , Boltzmann constant), denoting the correction of pH.

$\Delta G_{\text{U}} = -neU$ , where U is the electrode applied potential relative to reversible hydrogen electrode (RHE) and n is the number of electrons transferred. The ORR reaction under

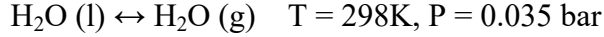
acid condition can be written as:



The ORR reaction can be viewed as a four-step elemental reaction:



In the standard hydrogen electrode (pH=0, T=298 K), the free energy of the solvated proton and electron pair ( $\text{H}^+ + \text{e}^-$ ) can be calculated as  $1/2G(\text{H}_2)$ . Zero-point energy can be calculated using vibrational frequencies by applying normal-mode analysis through DFT calculations. For gas phase free molecules ( $\text{H}_2\text{O}$ ,  $\text{H}_2$ ), the entropy was taken from NIST database, and the entropy of intermediates (\*OOH, \*O, \*OH) were omitted and considered equal to 0. The value of  $G(\text{H}_2\text{O} (l))$  was calculated according to the following equilibrium:



Because DFT calculations cannot accurately describe the high-spin ground state of oxygen molecule, the Gibbs free energy of  $\text{O}_2$  can be obtained indirectly by  $G(\text{O}_2) = 2G(\text{H}_2\text{O}) - 2G(\text{H}_2) + 4.92 \text{ (eV)}$ . Therefore, the free energy change of each step in the reaction equation can be written as:

$$\Delta G_1 = G_{* \text{OOH}} - (G_* + G_{\text{O}_2} + 1/2G_{\text{H}_2}) \quad (\text{S2})$$

$$\Delta G_2 = G_{* \text{O}} + G_{\text{H}_2\text{O}} - (G_{* \text{OOH}} + 1/2G_{\text{H}_2}) \quad (\text{S3})$$

$$\Delta G_3 = G_{* \text{OH}} - (G_{* \text{O}} + 1/2G_{\text{H}_2}) \quad (\text{S4})$$

$$\Delta G_4 = G_* + G_{\text{H}_2\text{O}} - (G_{* \text{OH}} + 1/2G_{\text{H}_2}) \quad (\text{S5})$$

Meanwhile, the adsorption free energy of \*OOH, \*O, \*OH is defined as follows:

$$\Delta G_{* \text{OOH}} = G_{* \text{OOH}} - G_* - (2G_{\text{H}_2\text{O}} - 3/2G_{\text{H}_2}) \quad (\text{S6})$$

$$\Delta G_{* \text{O}} = G_{* \text{O}} - G_* - (G_{\text{H}_2\text{O}} - G_{\text{H}_2}) \quad (\text{S7})$$

$$\Delta G_{* \text{OH}} = G_{* \text{OH}} - G_* - (G_{\text{H}_2\text{O}} - 1/2G_{\text{H}_2}) \quad (\text{S8})$$

In this way, the free energy change of each step can be expressed in terms of the free energy of the intermediate adsorption:<sup>4</sup>

$$\Delta G_1 = \Delta G_{*_{\text{OOH}}} - 4.92 \quad (\text{S9})$$

$$\Delta G_2 = \Delta G_{*_{\text{O}}} - \Delta G_{*_{\text{OOH}}} \quad (\text{S10})$$

$$\Delta G_3 = \Delta G_{*_{\text{OH}}} - \Delta G_{*_{\text{O}}} \quad (\text{S11})$$

$$\Delta G_4 = -\Delta G_{*_{\text{OH}}} \quad (\text{S12})$$

Of the above four steps, the step with the most difficult energy climb determines the reaction rate and is called the potential-determining step (PDS). To describe the catalytic performance, the overpotential is defined as:

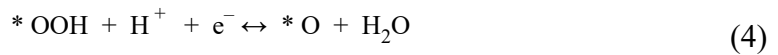
$$\eta_{\text{ORR}} = \frac{\max(\Delta G_1, \Delta G_2, \Delta G_3, \Delta G_4)}{e} + 1.23 \quad (\text{S13})$$

## Microkinetic model

In the microkinetic model, the reaction pathway and rate constant of the elementary reaction need to be determined. After that, we can solve a set of ordinary differential equations (ODEs) at steady state. By solving ODEs, we can obtain the information about the coverage of intermediates and turnover of frequency (TOF) of electrons.

## Reaction pathway

The ORR reaction pathway at TM@gra involving six elementary reaction steps:



where the (1), (2) is nonelectrochemical step, and the rest is electrochemical step.

## Rate constant

For nonelectrochemical step, the rate constant ( $k_i$ ) and equilibrium constants ( $K_i$ ) are given by:

$$k_i = v_i \exp\left(-\frac{E_a}{k_B T}\right) \quad (\text{S14})$$

$$K_i = \exp\left(-\frac{\Delta G_i}{k_B T}\right) \quad (\text{S15})$$

For electrochemical step, they are given by:

$$k_i = A_i \exp\left(-\frac{E_{a,i}}{k_B T}\right) \exp\left(-\frac{e\beta_i(U - U_i)}{k_B T}\right) \quad (\text{S16})$$

$$K_i = \exp\left(-\frac{\Delta G_i + eU}{k_B T}\right) \quad (\text{S17})$$

$$U_i = -\frac{\Delta G_i}{e} \quad (\text{S18})$$

$$k_{-i} = \frac{k_i}{K_i} \quad (\text{S19})$$

where the  $G_i$ ,  $E_a$  and  $A_i$  are the free energy change, activation energy and pre-exponential factor, respectively. The activation energy of electrochemical step is estimated as 0.28 eV due to solvent reorganization, and  $A_i$  is estimated as  $1.23 \times 10^9 \text{ s}^{-1}$ .  $\beta_i$  is symmetric factor taken as 0.5. The values of factors ( $A_i$ ,  $\beta_i$ ) and  $E_a$  for proton transfer are taken from the reference,<sup>5</sup> and the  $G_i$  of all steps are calculated by DFT.

## Rate differential equations

Based on the part of reaction pathway and rate constant, the rate differential equations can be given at steady state as follows:

$$\frac{\partial x_{\text{O}_2}(\text{dl})}{\partial t} = k_1 x_{\text{O}_2}(\text{aq}) - k_{-1} x_{\text{O}_2}(\text{dl}) - k_2 x_{\text{O}_2}(\text{dl}) \theta_* + k_{-2} \theta_* \text{O}_2 \quad (\text{S20})$$

$$\frac{\partial \theta_*}{\partial t} = -k_2 x_{\text{O}_2}(\text{dl}) \theta_* + k_{-2} \theta_* \text{O}_2 + k_6 \theta_* \text{OH} - k_{-6} \theta_* \text{H}_2\text{O} \quad (\text{S21})$$

$$\frac{\partial \theta_* \text{O}_2}{\partial t} = k_2 x_{\text{O}_2}(\text{dl}) \theta_* - k_{-2} \theta_* \text{O}_2 - k_3 \theta_* \text{O}_2 + k_{-3} \theta_* \text{OOH} \quad (\text{S22})$$

$$\frac{\partial \theta_{*OOH}}{\partial t} = k_3 \theta_{*O_2} - k_{-3} \theta_{*OOH} - k_4 \theta_{*OOH} + k_{-4} \theta_{*O} x_{H_2O} \quad (S23)$$

$$\frac{\partial \theta_{*O}}{\partial t} = k_4 \theta_{*OOH} - k_{-4} \theta_{*O} x_{H_2O} - k_5 \theta_{*O} + k_{-5} \theta_{*OH} \quad (S24)$$

$$\frac{\partial \theta_{*OH}}{\partial t} = k_5 \theta_{*O} - k_{-5} \theta_{*OH} - k_6 \theta_{*OH} + k_{-6} \theta_{*O} x_{H_2O} \quad (S25)$$

$$\theta_{*} + \theta_{*O_2} + \theta_{*OOH} + \theta_{*O} + \theta_{*OH} = 1 \quad (S26)$$

In these equations  $x_{H_2O} = 1$  and  $x_{O_2}(\text{aq}) = 2.34 \times 10^{-5}$ , corresponding to 1 atm  $O_2$  (g) in equilibrium with  $O_2$  (aq), and the rate equations are solved numerically at steady state.

## Current density

The current density is calculated as:

$$j = e \rho \text{TOF}_{e^-} \quad (S27)$$

where  $e$  is the elementary charge and  $\rho$  is the surface density of active sites and  $\text{TOF}_{e^-}$  is the turnover frequency of electrons. The value of  $e\rho$  is estimated as  $80.3 \mu\text{C}/\text{cm}^2$  based on the assumption that the surface density of active sites of TM@gra is the same as Pt(111)<sup>5</sup>.  $\text{TOF}_{e^-}$  can be given by solving above rate differential equations.

## Dynamic stability

The graphene adatom systems are generally unstable without doping or substitution. This instability is primarily due to the planar structure of graphene, where the  $p_z$  orbitals of the carbon atoms interact weakly with the metal atoms, leading to a tendency for metal atoms to aggregate. However, in fullerene the unique curved geometry plays a significant role in enhancing the binding of metal atoms.<sup>6-7</sup> Because the  $p_x$  and  $p_y$  orbitals extend into the external space due to the curvature of the surface. This makes the interaction between the metal atoms and the carbon framework more intense.

We performed detailed calculation of the diffusion barrier for metal atoms on the graphullerene surface by CI-NEB.<sup>8-9</sup> The process we focus is one Cr atom moving out from its ground state to the Cr next to it. The route diagram and related data are shown

in Fig. S9, and the result shows that the barrier is 1.12 eV. Consider Arrhenius process  $R = R_0 \exp(-E_b / k_B T)$ , if we take  $R_0 = 10^{13} \text{ s}^{-1}$ ,  $T = 300 \text{ K}$ , the transition rate is about  $R = 2.2 \times 10^{-6} \text{ s}^{-1}$ . This rate means the transition can be safely ignored in the macro-scale view. Similar results also can be found in calculations of Suo et al. in the same graphullerene structure.<sup>10</sup> We also compared our system with other materials. Similar studies have shown that high diffusion barriers (e.g., 0.56 eV for chromium atoms in Fe-Cr alloys) can effectively inhibit sintering.<sup>11</sup> Therefore, Our calculated potential barriers indicates that our model system is plausible and stable under the studied conditions.

### **Thermodynamic stability and corrosion resistance**

The minimum-energy path (MEP) calculated by CI-NEB reveals that the  $E_{\text{bar}}$  for a Cr single atom jumping between two neighboring sites is 1.22 eV (see Fig. S10). Clearly, such a substantial  $E_{\text{bar}}$  effectively hinders the diffusion of Cr atoms. To further dispel the misgivings, we additionally examine the thermodynamic stability of Cr@gra complex through ab initio molecular dynamics simulations at 300 K (see Fig. S11). The first 200 fs are used to allow the system to reach equilibrium so that data collection begins from 200 fs. The results suggest that the graphullerene network keeps stable at temperatures near 300 K, which is in line with the experimental result that the graphullerene network does not decompose at 600 K.<sup>12-13</sup>

We also examined the corrosion process of the system. First, the  $C_{60}$  system is stable in acidic environment which can be deduced from the paper,<sup>14</sup> in which the authors synthesized carbon nanotube/ $C_{60}$  and used it as a catalyst in acidic solution. Therefore, we focus on the stability of the Cr/graphullerene in acidic solution. The corrosion process is as follows:



Where \* denotes in the  $C_{60}$  network, because the hydrogen ion cannot be directly calculated in DFT, we use the DFT calculated energy of a hydrogen atom plus the ionization energy 13.6 eV as the energy of an isolated hydrogen ion. The hydration energy of a hydrogen ion is -11.3 eV.<sup>15</sup> The hydration energy of a  $\text{Cr}^{3+}$  is taken as an

experimental value  $-41.6$  eV.<sup>16</sup> All other values were computed with the PCM model implemented in VASP\_sol. By this way, we confirmed that the reaction needs extra  $11.6$  eV to proceed, which means difficult to happen.

### **Convergence test**

We use plane-wave as basis sets to expand the Hilbert space. For plane-wave, the basis set completeness is determined by the energy cutoff. Also, the K-point sampling is important for the accuracy.

To ensure the basis set completeness, we performed systematic convergence tests for ( $E_{\text{cutoff}}$ ). We calculated the energies of the materials at different cutoff energies and K-points ( $E_{\text{cutoff}}$  ranges from  $400$  to  $600$  eV, K-points are taken as  $3\times 2\times 1$ ,  $4\times 2\times 1$ ,  $7\times 4\times 1$ , etc.) (Figs. S13 and S14). At a cutoff energy of  $500$  eV and a K-point of  $4\times 2\times 1$ , the energy converges within  $1$  meV/atom, and the cutoff energy of  $500$  eV and the K-point grid of  $4\times 2\times 1$  were finally selected for subsequent calculations in order to balance the computational accuracy and efficiency.

### **Two reaction pathways**

We suppose only single site active process can happen because the large spacing of the four metal sites in the catalyst (the distance between the two nearest Cr atoms is about  $5$  Å) prevents the formation of multi-site synergies. Therefore, there is only one active site available, where  $\text{O}_2$  is stabilized on the substrate by side-on adsorption, allowing it to be activated efficiently.

Focusing on the single site active process, there are usually two reaction pathways in the ORR,<sup>17</sup> one is four-electron reaction which lead to formation of  $\text{H}_2\text{O}$ , the other is two-electron reaction which lead to formation of  $\text{H}_2\text{O}_2$ . Our Gibbs free energy calculations further confirm that after the first protonation step, the two-electron pathway generates  $\text{H}_2\text{O}_2$  as an endothermic process ( $\Delta G = +1.006$  eV), whereas the four-electron pathway is exothermic (as shown in Fig. S15). This thermodynamic difference clearly explains why the four-electron path is energetically more favorable and the two-electron process can be safely ignored.

### **Different active site reactions**

We carried out the analysis for a symmetric structure consisting of four metal atoms (labeled 1, 2, 3 and 4). As shown in Fig. S16a, the red dashed line divides the structure into upper and lower symmetric regions, and the metal atoms can be divided into two categories: site-I (1 and 4) and site-II (2 and 3). Through DFT calculations, we systematically evaluated the adsorption behaviors of oxygen molecules on different sites. The results showed that O<sub>2</sub> adsorbed at site-II was energetically favorable ( $\Delta E = -0.246$  eV) compared to site-I. This thermodynamic preference led us to focus on the site-II-dominated ORR pathway. We further supplemented the calculation of the adsorption free energies of key intermediates (e.g., \*OOH, \*O and \*OH) on site-I. As shown in Fig. S16b, the adsorption free energies of each intermediate on site-I were higher than that on site-II (e.g.,  $\Delta G = -0.781$  eV for \*OOH at site-I and  $-0.841$  eV at site-II). The Gibbs free energy plot shows that the first protonation step as the potential-determining step for both sites, and site-I exhibits a higher overpotential (0.449 V) than site-II (0.389 V). The result further validates thermodynamically that site-II is justified as the main active site, and at the same time excludes the dominant role of site-I in ORR.

### **Determination of active site (metal atom or C atom)**

We performed extensive calculations on O<sub>2</sub> adsorption, considering various initial orientations, including several typical configurations of O<sub>2</sub> molecules near the C<sub>60</sub> structure (O<sub>2</sub> molecules in vertical, horizontal, and tilted orientations). Here, we show the initial and optimized structures in Fig. S17, using Cr as a typical example. In the initial structure, the O<sub>2</sub> molecules are positioned about 1.5 Å from a C atom of C<sub>60</sub> and about 2.5 Å from the Cr atom. After optimization, the O<sub>2</sub> molecules adsorb onto the metal site. As shown in Fig. S17, the O<sub>2</sub> molecule automatically relaxes to the Cr site even if we manually place it near C<sub>60</sub>. It can be concluded that the metal atom is the active site of the ORR catalyzed reaction.

### **References**

- (1) Lin, C.; Yin, G.; Zhao, Y. Calculation of the Cohesive Energy of Solids with the Use of Valence Electron Structure Parameters. *Comput. Mater. Sci.* **2015**, *101*, 168-174.
- (2) Mardiyah, R. U.; Arkundato, A.; Misto; Purwandari, E. Energy Cohesive Calculation for Some

Pure Metals Using the Lennard-Jones Potential in Lammmps Molecular Dynamics. *J. Phys. Conf. Ser.* **2020**, *1491*, 012020.

(3) Norskov, J. K.; Rossmeisl, J.; Logadottir, A.; Lindqvist, L.; Kitchin, J. R.; Bligaard, T.; Jónsson, H. Origin of the overpotential for oxygen reduction at a fuel-cell cathode. *J. Phys. Chem. B* **2004**, *108*, 17886-17892.

(4) Zhang, X.; Yang, Z.; Lu, Z.; Wang, W. Bifunctional CoN<sub>x</sub> embedded graphene electrocatalysts for OER and ORR: A theoretical evaluation. *Carbon* **2018**, *130*, 112-119.

(5) Hansen, H. A.; Viswanathan, V.; Nørskov, J. K. Unifying Kinetic and Thermodynamic Analysis of 2 e<sup>-</sup> and 4 e<sup>-</sup> Reduction of Oxygen on Metal Surfaces. *J. Phys. Chem. C* **2014**, *118*, 6706-6718.

(6) Xu, J. Z.; Bakker, J. M.; Lushchikova, O. V.; Lievens, P.; Janssens, E.; Hou, G. L. Pentagon, Hexagon, or Bridge? Identifying the Location of a Single Vanadium Cation on Buckminsterfullerene Surface. *J. Am. Chem. Soc.* **2023**, *145*, 22243-22251.

(7) Guan, R.; Chen, Z.-C.; Huang, J.; Tian, H.-R.; Xin, J.; Ying, S.-W.; Chen, M.; Zhang, Q.; Li, Q.; Xie, S.-Y.; Zheng, L.-S.; Yang, S. Self-Driven Carbon Atom Implantation into Fullerene Embedding Metal-Carbon Cluster. *Proc. Natl. Acad. Sci. U. S. A.* **2022**, *119*.

(8) Henkelman, G.; Jónsson, H. Improved Tangent Estimate in the Nudged Elastic Band Method for Finding Minimum Energy Paths and Saddle Points. *J. Chem. Phys.* **2000**, *113*, 9978-9985.

(9) Henkelman, G.; Uberuaga, B. P.; Jónsson, H. A Climbing Image Nudged Elastic Band Method for Finding Saddle Points and Minimum Energy Paths. *J. Chem. Phys.* **2000**, *113*, 9901-9904.

(10) Suo, H.; Li, M.; Yang, G.; Du, Y.; Zhao, X.; Ren, X.; Li, S. Covalent-Bond-Linked Monolayer Fullerene Network as a Spin Sponge for Spin-Triplet O<sub>2</sub> Activation and CO Oxidation. *Phys. Rev. B* **2024**, *110*, 125405.

(11) Chen, D.; Gao, F.; Hu, W. Y.; Hu, S. Y.; Terentyev, D.; Sun, X.; Heinisch, H. L.; Henager, C. H.; Khaleel, M. A. Migration of Cr-Vacancy Clusters and Interstitial Cr in  $\alpha$ -Fe Using the Dimer Method. *Phys. Rev. B* **2010**, *81*, 064101.

(12) Peng, B. Monolayer Fullerene Networks as Photocatalysts for Overall Water Splitting. *J. Am. Chem. Soc.* **2022**, *144*, 19921-19931.

(13) Hou, L.; Cui, X.; Guan, B.; Wang, S.; Li, R.; Liu, Y.; Zhu, D.; Zheng, J. Synthesis of a Monolayer Fullerene Network. *Nature* **2022**, *606*, 507-510.

(14) Gao, R.; Dai, Q.; Du, F.; Yan, D.; Dai, L. C<sub>60</sub>-Adsorbed Single-Walled Carbon Nanotubes as Metal-Free, pH-Universal, and Multifunctional Catalysts for Oxygen Reduction, Oxygen Evolution, and Hydrogen Evolution. *J. Am. Chem. Soc.* **2019**, *141*, 11658-11666.

(15) Palascak, M. W.; Shields, G. C. Accurate Experimental Values for the Free Energies of Hydration of H<sup>+</sup>, OH<sup>-</sup>, and H<sub>3</sub>O<sup>+</sup>. *J. Phys. Chem. A* **2004**, *108*, 3692-3694.

(16) Kepp, K. P. Thermochemically Consistent Free Energies of Hydration for Di- and Trivalent Metal Ions. *J. Phys. Chem. A* **2018**, *122*, 7464-7471.

(17) Kulkarni, A.; Siahrostami, S.; Patel, A.; Norskov, J. K. Understanding Catalytic Activity Trends in the Oxygen Reduction Reaction. *Chem. Rev.* **2018**, *118*, 2302-2312.